Depletion potentials in highly size-asymmetric binary hard-sphere mixtures: Comparison of simulation results with theory

Douglas J. Ashton,[1] Nigel B. Wilding,[1] Roland Roth,[2] and Robert Evans[3]
[1]*Department of Physics, University of Bath, Bath BA2 7AY, United Kingdom*
[2]*Institut für Theoretische Physik, Universität Erlangen-Nürnberg, Staudtstrasse 7, D-91058 Erlangen, Germany*
[3]*H. H. Wills Physics Laboratory, University of Bristol, Royal Fort, Bristol BS8 1TL, United Kingdom*
(Received 15 September 2011; published 20 December 2011)

We report a detailed study, using state-of-the-art simulation and theoretical methods, of the effective (depletion) potential between a pair of big hard spheres immersed in a reservoir of much smaller hard spheres, the size disparity being measured by the ratio of diameters $q \equiv \sigma_s/\sigma_b$. Small particles are treated grand canonically, their influence being parameterized in terms of their packing fraction in the reservoir η_s^r. Two Monte Carlo simulation schemes—the geometrical cluster algorithm, and staged particle insertion—are deployed to obtain accurate depletion potentials for a number of combinations of $q \leqslant 0.1$ and η_s^r. After applying corrections for simulation finite-size effects, the depletion potentials are compared with the prediction of new density functional theory (DFT) calculations based on the insertion trick using the Rosenfeld functional and several subsequent modifications. While agreement between the DFT and simulation is generally good, significant discrepancies are evident at the largest reservoir packing fraction accessible to our simulation methods, namely, $\eta_s^r = 0.35$. These discrepancies are, however, small compared to those between simulation and the much poorer predictions of the Derjaguin approximation at this η_s^r. The recently proposed morphometric approximation performs better than Derjaguin but is somewhat poorer than DFT for the size ratios and small-sphere packing fractions that we consider. The effective potentials from simulation, DFT, and the morphometric approximation were used to compute the second virial coefficient B_2 as a function of η_s^r. Comparison of the results enables an assessment of the extent to which DFT can be expected to correctly predict the propensity toward fluid-fluid phase separation in additive binary hard-sphere mixtures with $q \leqslant 0.1$. In all, the new simulation results provide a fully quantitative benchmark for assessing the relative accuracy of theoretical approaches for calculating depletion potentials in highly size-asymmetric mixtures.

DOI: 10.1103/PhysRevE.84.061136 PACS number(s): 64.60.De, 64.75.Xc, 64.75.Cd, 05.10.Ln

I. INTRODUCTION

Much of condensed matter physics and chemistry is concerned with simplifying the description of a complex many-body system by integrating out certain subsets of the degrees of freedom of the full system. Thus in treating atomic and molecular solids and liquids one often resorts to integrating out, usually approximately, the higher energy quantum mechanical degrees of freedom of the electrons in order to obtain an effective interatomic or intermolecular potential energy function that is then employed in a classical statistical mechanical treatment to study the properties of condensed phases. Similarly in metallic systems integrating out the degrees of freedom of the conduction electrons leads to an effective Hamiltonian for the screened ions or pseudo-atoms. When one turns to complex, multicomponent fluids such as colloidal suspensions or polymers in solution the basic idea is similar: One integrates out the degrees of freedom of the small species to obtain an effective Hamiltonian for the biggest species; for an illuminating review see Ref. [1]. In this case all species can be treated classically, and the formalism is essentially the famous one of McMillan and Mayer [2], who developed a general theory for the equilibrium properties of solutions. These authors and many others subsequently recognized that integrating out is best performed when the smaller species (those constituting the solvent) are treated grand canonically. Obtaining the full effective Hamiltonian is a tall order. A first step in any theoretical treatment is to determine the effective potential between a single pair of the biggest particles in a sea of the smaller species. There is a long history of work in this field. Various statistical mechanical techniques have been developed to calculate these potentials for different types of complex fluid. Well-known examples of effective two-body potentials, forming cornerstones of colloid science, are the Derjaguin-Landau-Verwey-Overbeek (DLVO) potential for charged colloids and the Asakura-Oosawa depletion potential for colloid-polymer mixtures. Further examples, including polymer systems, are given in Refs. [1,3].

The problem of determining the effective two-body interaction is particularly challenging to theory and computer simulation in the situation where—and we specialize to a binary fluid—the bigger particles are much larger than the smaller ones. Sophisticated theoretical and simulation techniques, which will provide accurate results for the effective potential, are only now becoming available.

Our present focus is on a simple model for a suspension of a binary mixture of big and small colloidal particles, both species suitably sterically stabilized; i.e., we consider a highly size asymmetric binary mixture of hard spheres. This can also serve as a crude model of a mixture of colloids and nonadsorbing polymer and can be regarded as a reference system for a mixture of size asymmetric simple fluids.[1] The hard-sphere

[1]It is not universally accepted that a binary mixture of hard spheres is a good reference system for binary mixtures of colloids in suspensions. Residual (non-hard-sphere) interactions might play

mixture is important in that it provides a testing ground for theories of the effective potential between two big hard spheres immersed in reservoirs of small ones, with different packing fractions η_s^r, and, indeed, for theories of the full effective Hamiltonian obtained when the degrees of freedom of the small species are integrated out fully [4]. Generally speaking, the more asymmetric the mixture the more difficult it is to treat both species on equal footing and the more necessary it is to perform some integrating out to obtain an (approximate) effective Hamiltonian. Often this procedure is feasible only at the level of a Hamiltonian consisting of a sum of (effective) pair potentials, as obtained by considering a single pair of the big particles, along with zero- and one-body terms [1,4]. One of the advantages of the hard-sphere system is that geometrical considerations indicate that three-, four-, etc., body terms become less important as the size ratio $q = \sigma_s/\sigma_b$ becomes small. Here σ_s and σ_b denote the diameters of the small and big species, respectively. Thus provided one can calculate an accurate effective pair potential, the pair description alone determines an effective Hamiltonian that should provide an excellent description of the big-big correlation functions and the phase behavior of the binary hard-sphere mixture when q is sufficiently small [4]. Note that in this paper we consider additive hard-sphere mixtures so that the big-small diameter $\sigma_{bs} = (\sigma_b + \sigma_s)/2$.

Since the studies of the phase behavior of the hard-sphere mixture by Dijkstra *et al.* [4], whose simulations of an effective one-component system used a rather crude approximate pair potential, there have been several new developments in the theory of effective potentials. Most of these are based on Density Functional Theory (DFT). It is important to assess whether (1) the potentials derived in recent studies are accurate and (2) use of these might lead to different predictions for the properties of the mixture. In order to make such assessments it is necessary to have accurate simulation results for the effective potential. Employing state-of-the art techniques we provide what we believe are the most accurate results currently available for $q \leqslant 0.1$ and packing fractions η_s^r up to 0.35 and make direct comparisons with the results of theoretical approaches. The simulation techniques we employ do not allow us to work at very high values of η_s^r, but they do allow us to compute accurate effective potentials, for a range of size ratios, in the regime of small sphere packing fractions where the putative (metastable) fluid-fluid phase separation is predicted to occur [4]. By calculating the second virial coefficient associated with the effective potential we make new estimates of the value of η_s^r where the onset of this elusive phase transition occurs. Of course, real colloidal systems may not reach equilibrium on experimental time scales, particularly if the effective potential exhibits significant repulsive barriers [5]. Nevertheless, knowledge of the underlying phase behavior is important for interpreting dynamical observations, such as whether gelation or glassiness might set in Refs. [6,7].

The comparison between DFT results and simulation addresses recent suggestions [8,9] that no existing theoretical framework is reliable for calculating effective potentials for small values of q and physically relevant values of η_s^r. We examine and refute these suggestions in the light of our present results.

The effective potential between two big hard spheres takes the form

$$\phi_{\rm eff}(r_{bb}) = \phi_{bb}(r_{bb}) + W(r_{bb}), \tag{1}$$

where ϕ_{bb} is the bare hard-sphere potential between two big spheres and W is the so-called depletion potential. This is attractive for small separations r_{bb} of the big spheres but decays in an exponentially damped oscillatory fashion at large separations. The physics of the attraction is well understood: The exclusion or depletion of the small spheres as the big ones come close together results in an increase in free volume available to the small species leading to an increase of entropy. If this attraction is sufficiently strong it can give rise to fluid-fluid phase separation. Such a phase transition is driven by purely entropic effects: Recall that all the bare interactions in the mixture are those of hard spheres. Of course, the concept of an attractive depletion potential between colloids dispersed in a solution of nonadsorbing polymer or other depletants has a long history. The recent book by Lekkerkerker and Tuinier [10] describes this and the general importance of depletion interactions in colloidal systems.

We have emphasized that the effective pair potential is a key ingredient in an effective Hamiltonian description of the mixture. However, this object is also important in its own right since it can be measured experimentally for colloidal systems using various techniques. More specifically, the effective potential between a single colloid, immersed in a suspension of small colloidal particles or nonadsorbing polymer, and a flat substrate has been measured; see, for example, Ref. [11] and the comparisons made between DFT results and experiment [12]. Crocker *et al.* [13] measured the effective potential between two big PMMA particles immersed in a sea of small polystyrene spheres and observed damped oscillations at high small-sphere packing fractions. Subsequently comparisons were made with DFT results [14]. Reference [15] provides a recent review of direct experimental measurements of effective interactions in colloid-polymer systems.

A. Previous simulation studies

In general, the task of accurately measuring effective potentials in highly size-asymmetrical fluid mixtures using traditional simulation methods such as molecular dynamics (MD) or Monte Carlo (MC) is an extremely challenging one. The difficulty stems from the slow relaxation of the big particles caused by the presence of the small ones. Specifically, in order for a big particle to relax, it must move a distance of order its own diameter σ_b. However, for small size ratios q, and even at quite low values of η_s^r, very many small particles are typically to be found surrounding a big particle, and these hem it in, greatly hindering its movement. In computational terms this mandates a very small MD time step in order to control integration errors, while in MC simulations that employ local particle displacments, a very small trial step size must be used in order to maintain a reasonable acceptance rate. Consequently, the computational investment required to simulate highly size-asymmetric mixtures by traditional means

a role in determining the effective big-big potential and the phase behavior. See, e.g., Ref. [62] and references therein.

is (generally speaking) prohibitive at all but the lowest packing fractions of small particles.

Owing to these difficulties, most previous simulation studies of hard-sphere mixtures [8,9,16–18] have adopted an indirect route to measuring effective potentials in the highly size-asymmetrical regime $q \leqslant 0.1$ based on measurements of interparticle *force*. The strategy rests on the observation that the force between two big particles can be expressed in terms of the contact density of small particles at the surface of the big ones [17,19]. By measuring this (angularly dependent) contact density for fixed separation r_{bb} of the big particles and repeating for separations ranging from the minimum value $r_{bb} = \sigma_b$ to $r_{bb} = \infty$, one obtains the force profile $F(r_{bb})$. This can in turn be integrated to yield an estimate of the depletion potential. Generally speaking, however, the statistical quality of the data obtained via this route seems typically quite low, particularly at small q and high η_s^r. This presumably reflects the difficulties of measuring contact densities accurately and the errors inherent in numerical integration.

Only a few studies have tried to measure the depletion potential directly for $q \leqslant 0.1$ (see Refs. [20,21] for hard-sphere studies and Refs. [22,23] for more general potentials). In common with the present work, these studies deployed a cluster algorithm (to be described in Sec. II A) to deal efficiently with the problem of slow relaxation outlined above. However, they treated the small particles canonically rather than grand canonically, which complicates comparison with theoretical predictions, which are typically formulated in terms of an infinite reservoir of small particles.[2] Furthermore it seems that no previous simulation studies have discussed (in any detail) finite-size effects in measurements of depletion potentials, the role of which we believe to be particularly significant at large size asymmetries. Consequently, while previous work has evidenced good qualitative agreement between simulation and theory, there is to date a lack of data from which one can make confident comparisons between the various theoretical approaches. This is remedied in the present work.

B. Previous theoretical studies

There are many of these, and they are based on a variety of techniques. Integral equation treatments abound, and some of these are summarized in the recent article by Boţan *et al.* [24]. The studies of Amokrane and co-workers that implement sophisticated closure approximations within a bridge functional approach probably constitute the state of the art in integral equation treatments of asymmetric mixtures; see, e.g., Refs. [25,26]. A related rational function approach was used recently by Yuste *et al.* [27]. Tackling highly asymmetric mixtures via integral equation methods, where one treats both species on equal footing, is notoriously difficult, and making systematic assessments of the reliability of closure approximations is not straightforward and, of course, requires accurate simulation data.

Density functional (DFT) treatments are arguably much more powerful. There are several different ways of calculating the effective (depletion) potential between two big hard spheres in a reservoir of small hard spheres or more generally of calculating the effective potential between two big particles in a reservoir of small ones with arbitrary interactions between *bb, bs,* and *ss*. The first method is to fix the centers of the big (b) particles a distance r_{bb} apart and then compute the grand potential of the small (s) particles in the external field of the two fixed b particles as a function of r_{bb} for a given size ratio q and a reservoir packing fraction of η_s^r. This method requires only a DFT for a single-component fluid, the small particles. The big particles are fixed so they simply exert an external potential on the small ones. DFT for one-component hard spheres is very well developed; very accurate functionals exist, and these are suitable for treating the extreme inhomogeneities that arise for small size ratios q. It follows that this brute force method should be rather accurate. Its drawback is that the density profile of the small particles has cylindrical symmetry requiring numerically accurate minimization of the free energy functional on a two-dimensional grid.

Goulding [30,31] performed pioneering brute force calculations using the Rosenfeld fundamental measure theory (FMT) [30] for a system with $q = 0.2$ and packing fractions η_s^r up to 0.314. This method has been refined recently by Boţan *et al.* [24] who employed various hard-sphere functionals for more asymmetric systems and higher values of η_s^r. These authors (see also Oettel *et al.* [31]) also used DFT to calculate the depletion force directly using the formula due to Attard [17,19] that relates the force to the density profile of small spheres in contact with a big sphere. Once again the density profile has cylindrical symmetry, and careful numerical methods are required.

A popular DFT method for hard-sphere systems is based on what has become known as the insertion trick or insertion method [14,18]. This is a general procedure (see Sec. III A) for calculating the depletion potential between a big particle and a fixed object, e.g., a wall or another big particle, immersed in a sea of small particles. The advantage of the method is that one requires only the equilibrium density profile of the small species in the external field of the isolated fixed object, and this profile clearly has the symmetry of the single fixed object. For the case of two big spheres the profile $\rho_s(r)$ has spherical symmetry. The disadvantage is that the theory requires a DFT for an asymmetric mixture, albeit in the limit where the density ρ_b of the big particles approaches zero: $\rho_b \to 0$. For hard-sphere mixtures the insertion method is straightforward to implement, and Ref. [14] provides a series of comparisons, using the Rosenfeld FMT [30], with the simulation data that existed in 2000.

Further comparisons between results of the DFT insertion method and simulation studies were made in Refs. [8,9,24, 31]. In the present paper we seek to make more quantitative comparisons, taking into consideration the improved accuracy of our new simulation results and the availability of improved DFTs for hard-sphere fluids.

There is a further theoretical approach to calculating depletion potentials developed very recently in Ref. [31] and employed subsequently in Ref. [24]. This approach is based on morphological (or morphometric) thermodynamics [32]. The basic idea is that the depletion potential is (essentially) the solvation free energy of the dumbbell formed by the

[2]However, see Ref. [18] for a grand canonical study at $q = 0.2$.

two big spheres and that this quantity can be separated into geometrical measures, namely, the volume, surface area, and integrated mean and Gaussian curvatures. The coefficients of these measures are geometry-independent thermodynamic quantities, i.e., the pressure, the planar surface tension, and two bending rigidities, all of which can be obtained from simulations or from DFT calculations of the single-component fluid performed for a simple geometry.

The paper is arranged as follows: Sec. II describes the grand canonical simulation methods that we have employed for determining the depletion potential between two big spheres for size ratios q from 0.1 to 0.01. In Sec. III we summarize briefly the DFT insertion method and the three hard-sphere functionals that we employ in our present calculations. We also discuss some of the limitations of the parametrization of the depletion potential introduced in Ref. [14]. Some details of the morphometric approaches are also given here. Results are presented in Sec. IV. As a test of our simulation method we determine the depletion potential for two big hard spheres in a solvent of noninteracting point particles that have a hard interaction with the big spheres. For this case the depletion potential is known analytically; it is the venerable Asakura-Oosawa potential [33,34] of colloid science. For the additive binary hard-sphere case we make comparisons between results of simulation, DFT insertion method, the morphometric approach, and the Derjaguin approximation [35] for the depletion potential. We also compare simulation, DFT, and morphometric results for the associated second virial coefficient $B_2(\eta_s^r)$. The latter provides a valuable indicator of the propensity of the bulk binary mixture to phase separate into two fluid phases [36,37]. We conclude in Sec. V with a discussion.

II. SIMULATION METHODS

A. Geometrical cluster algorithm

An efficient cluster algorithm capable of dealing with hard spheres mixtures was introduced by Dress and Krauth in 1995 [38]. It was subsequently generalized to arbitrary interaction potentials by Liu and Luijten [22,39], who dubbed their method the Geometrical Cluster Algorithm (GCA). Here we describe the application of the GCA to a size asymmetrical binary mixture of hard spheres.

The particles comprising the system are assumed to be contained in a periodically replicated cubic simulation box of volume V. The configuration space of these particles is explored via cluster updates, in which a subset of the particles known as the "cluster" is displaced via a point reflection operation in a randomly chosen pivot point. The cluster generally comprises both big and small particles, and by virtue of the symmetry of the point reflection, members of the cluster retain their relative positions under the cluster move. Importantly, cluster moves are rejection-free even for arbitrary interparticle interactions [22]. This is because the manner in which a cluster is built ensures that the new configuration is automatically Boltzmann distributed.

For hard spheres, the cluster is constructed as follows: One of the particles is chosen at random to be the seed particle of the cluster. This particle is point-reflected with respect to the pivot from its original position to a new position. However, in its new position, the seed particle may overlap with other particles. The identities of all such overlapping particles are recorded in a list or "stack." One then takes the topmost particle off the stack and reflects its position with respect to the pivot. Any particles that overlap with this particle at its destination site are then added to the bottom of the stack. This process is repeated iteratively until the stack is empty and there are no more overlaps.

In this work we shall be concerned with measurements of the radial distribution function $g_{bb}(r)$ for a system containing a pair of big particles among many small ones. To effect this measurement we modify the GCA slightly as follows: We choose one big particle to be the seed particle, which we place uniformly at random within a shell $\sigma_{bb} < r < L/2$, centered on the second big particle, with L the linear box dimension. The location of the pivot is then inferred from the old and new positions of the seed particle. Thereafter clusters are built in the standard way. This strategy satisfies detailed balance and improves efficiency by ensuring that we generate only separations of the big particles that lie in the range $r = [\sigma_{bb}, L/2]$ for which $g_{bb}(r)$ is defined for hard spheres in a cubic box. The correctness of this technique was checked by comparing with the standard GCA approach described above.

Small particles are treated grand canonically in our simulations. In practical terms this means that in parallel with the cluster moves, we implement insertions and deletions of small particles, subject to a Metropolis acceptance criterion governed by an imposed chemical potential. The choice of chemical potential controls the reservoir packing fraction of small particles.

For the systems of interest in this work, we find that the GCA is efficient for reservoir packing fractions $\eta_s^r \lesssim 0.2$. Above this value one finds that practically all the particles join the cluster, which merely results in a trivial point reflection of the entire system. For single-component fluids this problem can be ameliorated by biasing the choice of pivot position to be close to the position of the seed particle [22]. Doing so has been reported to extend the operating limit to $\eta_s^r \simeq 0.34$. However, for the case of highly asymmetrical mixtures we find that this strategy does not significantly decrease the number of particles in the cluster because as soon as a second big particle joins the cluster and is point reflected it causes many overlaps with small particles.

B. Staged insertion algorithm

Our second MC approach for obtaining effective potentials for size asymmetrical mixtures is based on the staged insertion of a big particle [40–43]. The method involves first fixing one big particle at the origin and then sampling the free-energy change associated with inserting a second big particle at a prescribed distance r_{bb} from the origin. Essentially this amounts to an estimation of the chemical potential of the second particle $\mu_{ex}(r_{bb})$. As such our approach is close in spirit to one proposed very recently by Mladek and Frenkel [44], although their implementation did not employ staged insertion and was therefore restricted to low-density systems or those interacting via very soft potentials.

The effective potential for big particle separation r_{bb} is simply

$$W(r_{bb}) = \mu_{\rm ex}(r_{bb}) + C, \tag{2}$$

where the additive constant

$$C = -\lim_{r_{bb}\to\infty} \mu_{\rm ex}(r_{bb}) \tag{3}$$

can be determined as the excess chemical potential of a single big particle in the reservoir of small particles. To estimate $\mu_{ex}(r_{bb})$ we follow the strategy described in Ref. [42]. In outline, one imagines that the second big particle can exist in one of M possible "ghost" states in which it interacts with a small hard particle (a distance r_{bs} away) via the potential

$$\beta\phi_g^{(m)}(r_{bs}) = -[1 - \Theta(r_{bs} - \sigma_b)] \ln \lambda^{(m)} .$$

Here $m = 1, \ldots, M$ (an integer) indexes the ghost states, while the associated coupling parameter $0 \leqslant \lambda^{(m)} \leqslant 1$ controls the strength of the repulsion between the big particle and the small one. Owing to the step function Θ, the potential is uniformly repulsive over the volume of the big particle, and zero elsewhere. Moreover, for $\lambda^{(m)} > 0$ the repulsion is *finite* so that overlaps between small particles and the big one can occur. If we denote by N_o the number of such overlaps at any given time, then the configurational energy associated with the ghost big particle is

$$\beta\Phi_g^{(m)} = -N_o \ln \lambda^{(m)}. \tag{4}$$

Clearly for $\lambda^{(m)} = 0$, the big particle acts like a normal hard sphere, while for $\lambda^{(m)} = 1$ there is no interaction and the big particle is effectively absent from the system. To span this range we set the extremal states $\lambda^{(1)} = 0$ and $\lambda^{(M)} = 1$ and define some number of intermediate states that facilitate efficient MC sampling over the range $m = 1, \ldots, M$, i.e., that permits the ghost particle to fluctuate between being a real hard sphere and being absent. The measured value of the relative probability of finding the system in these extremal states yields the excess chemical potential:

$$\mu_{\rm ex}(r_{bb}) = \ln\left[\frac{p(\lambda^{(M)})}{p(\lambda^{(1)})}\right]. \tag{5}$$

Now since $W(r_{bb})$ is spherically symmetric, it can be estimated from Eqs. (5) and (2), by measuring $\mu_{\rm ex}(r_{bb})$ for values of $r_{bb} \geqslant \sigma_b$ along a one-dimensional grid. Moreover since each such measurement is independent of the others, the approach is trivially parallel and thus can be effectively farmed out on multicore processors.

Details of a suitable Metropolis scheme for sampling the full range of $m = 1, \ldots, M$ have been described in detail previously [42,43]. The basic idea is to perform grand canonical simulation of the small particles, supplemented by MC updates that allow transitions $m \to m \pm 1$ for the ghost big particle. These transitions are accepted or rejected on the basis of the change in the configurational energy Eq. (4). However, for this strategy to realize the aim of sampling the relative probability of the extremal states, it is necessary to bias the transitions such as to ensure approximately uniform sampling of the M ghost states. This is achieved by determining a suitable set of weights that appear in the MC acceptance probability [45].

Additionally it is important to choose sufficient intermediate states and to place them at appropriate values of λ such that transitions $m \to m \pm 1$ are approximately equally likely in both directions and have a reasonably high rate of acceptance. To achieve this we perform a preliminary run in which we consider a single big ghost particle in the reservoir of small ones. We first define $M = 1000$ values of λ in the range $(0,1)$, evenly spaced in $\ln\lambda$ and (in short runs) measure the distribution of overlaps $p(N_o|\lambda)$ for each. From this set we then pick out those values of λ for which successive $p(N_o|\lambda)$ exhibit an overlap by area of approximately 20%. This criterion yields a suitable set of intermediate states.

Efficiency benefits result from noting that the rate of transitions in m depends on how quickly the number of overlaps N_o relaxes after each successive transition. To enhance this relaxation we preferentially perform grand canonical insertions and deletions of small particles within a spherical subvolume of diameter $1.2\sigma_b$ centered on the second big particle. Updates within the subvolume occur with a frequency 100-fold that outside the subvolume. Our approach—which satisfies detailed balance—greatly reduces the time spent updating small particles whose coordinates are relatively unimportant for the quantity we wish to estimate.

The validity of the staged insertion technique was previously verified via comparisons with GCA in the context of grand canonical ensemble studies of phase behavior in highly size-asymmetrical binary mixtures of Lennard-Jones particles [43]. In the present context of hard-sphere depletion potentials, we have explicitly verified for $q = 0.1, \eta_s^r = 0.2$ that the staged insertion technique yields results that agree to within statistical errors with those determined using the GCA technique.

A further innovation, applicable to highly size-asymmetrical hard sphere mixtures, stems from the observation that it is not actually necessary to insert a big hard sphere in order to calculate the effective potential. Instead it is sufficient and (generally much more efficient) to insert a hard *shell* of infinitesimal thickness. The basic idea is that when fully inserted a hard shell particle encloses a number of small particles. These remain in equilibrium with the reservoir (i.e., their number can still fluctuate) but are fully screened from the rest of the system because their surfaces cannot penetrate the shell wall. Accordingly their contribution to the free energy is independent of the position of the shell particle, and hence their net effect is merely to shift the value of the additive constant in the measurement of $\mu_{\rm ex}(r_{bb})$. Since the latter is anyway set by hand to ensure that $\lim_{r_{bb}\to\infty} W(r_{bb}) = 0$, one does not need to know the contribution to the free energy from the enclosed particles.

From a computational standpoint, the task of inserting a hard shell is much less challenging than that of inserting a hard sphere: Essentially the chemical potential grows with the particle size ratio like $(1/q)^2$ rather than $(1/q)^3$. Consequently, far fewer intermediate stages M are required to effect the insertion, which reduces substantially the computational expenditure in measuring $\mu_{\rm ex}(r)$ accurately. We have explicitly verified that the shell insertion approach yields results for the effective potential that agree to within statistical error with those resulting from sphere insertion.

While the staged insertion technique is not as straightforward to implement as the GCA for highly asymmetrical

mixtures, it does not suffer the very rapid decrease in efficiency that renders the GCA inoperative for $\eta_s^r \gtrsim 0.2$. The computational expenditure required to obtain effective potentials via staged insertion does increase with η_s^r, but more gradually than for the GCA. Thus we were able to attain (for $q = 0.1$), the considerably larger reservoir packing fraction of $\eta_s^r = 0.35$. This was achieved for a computational expenditure of circa 2 weeks on a 150-core computing cluster, the bulk of which is associated with decorrelating the configurations of the small particles at this volume fraction. At the somewhat lower volume fraction of $\eta_s = 0.32$, only 2 days were required on the same machine. These figures sugest that while it may be feasible to go to somewhat higher volume fractions than $\eta_s = 0.35$, the computational cost would be high.

C. Correcting for finite-size effects

The effective potential $W(r)$ between two big particles is defined in terms of the radial distribution function $g(r) \equiv g_{bb}(r)$, with $r = r_{bb}$, measured in the limit of infinite dilution

$$-\beta W(r) = \lim_{\rho_b \to 0} \ln[g(r)]\,, \tag{6}$$

for $r > \sigma_b$. In our simulation studies this limit is approximated by placing a single pair of big hard spheres in the simulation box. A finite-size estimate to $g(r)$, which we shall denote $g_L(r)$, is then obtained by fixing the first of these particles at the origin and measuring (in the form of a histogram) the probability of finding the second big particle in a shell of radius $r \to r + dr$, i.e.,

$$g_L(r) = \frac{P(r)}{P_{\rm ig}(r)}\,, \tag{7}$$

where the normalization relates to the probability of finding an ideal gas particle at this radius:

$$P_{\rm ig}(r) = \frac{4\pi r^2}{V}\,. \tag{8}$$

Now, the principal source of finite-size error in $g_L(r)$ arises from the normalization of P_{ig} by the system volume. Specifically, for a finite-sized system, the volume occupied by the hard sphere at the origin is inaccessible to the second particle. Accordingly, the accessible system volume is

$$\tilde{V} = V - v_1, \tag{9}$$

where $v_1 = (1/6)\pi\sigma_b^3$ is the hard-sphere volume. More generally, one should define an *effective* excluded volume $\tilde{v}_1$ for use in Eq. (9), which allows for the fact that the small particles can mediate additional repulsions and/or attraction between the two big particles. In principle $\tilde{v}_1$ is given by

$$\tilde{v}_1 = 4\pi \int_0^\infty [1 - g(r)] r^2\, dr. \tag{10}$$

It follows from Eqs. (7)–(10) that the principal finite-size contribution to $g_L(r)$ is just an overall scale factor:

$$g(r) = \frac{\tilde{V}}{V} g_L(r)\,. \tag{11}$$

Accordingly $g_L(r)$ approaches $V/\tilde{V}$ at large r instead of unity, while the calculated effective potential, $W(r)$ decays to $\ln(\tilde{V}/V)$ instead of zero.

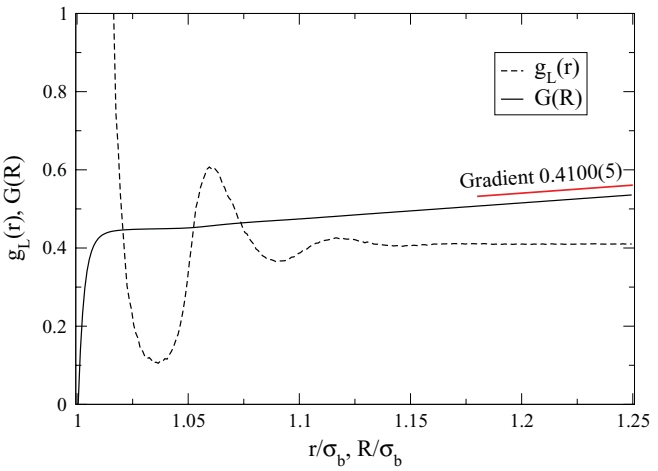

FIG. 1. (Color online) The measured form of $g_L(r)$ for $q = 0.05$, $\eta_s^r = 0.2$ obtained for a system size $L = 2.5\sigma_b$. Also shown is the cumulative integral $G(R) = \int_0^R g_L(r)\, dr$, together with an asymptotic linear fit, the gradient of which yields the finite-size correction factor for $g(r)$.

One can conceive of a number of possible approaches for dealing with this finite-size error. One is simply to minimize it by choosing a very large system volume V so that $V/\tilde{V}$ is close to unity. The disadvantage of this approach is that in a size-asymmetrical mixture, in which the big particles are in equilibrium with a reservoir of small ones, a huge number of small particles will necessarily fill the extra space available in a bigger box. All the interactions arising from these small particles then need to be computed, which can become prohibitively expensive.

Another route, which we have adopted in the present work, is to attempt to correct $g_L(r)$ by estimating the overall scale factor in Eq. (11), thus ensuring that $g(r) \to 1$ at large r. An expedient approach to doing so, which utilizes as much as possible of the information in $g_L(r)$, proceeds by determining the cumulative integral of $g_L(r)$:

$$G(R) = \int_0^R g_L(r)\, dr. \tag{12}$$

In practice, this integral was observed to tend toward a smooth linear form quite rapidly as the upper limit R increases, a fact illustrated for typical data in Fig. 1. A little thought then shows that if when left uncorrected $g(r)$ tends to $V/\tilde{V}$ at large r, the limiting gradient m of $G(R)$ is $m = V/\tilde{V}$, which thus provides the requisite correction factor for use in Eq. (11). Thus one corrects the measured histogram $g_L(r)$ by first fitting $G(R)$ to obtain an estimate of the limiting gradient of the linear part, and then scaling $g_L(r)$ according to $g(r) = m^{-1} g_L(r)$.

III. THEORETICAL METHODS

As mentioned in the Introduction we choose to make comparisons between our simulation results and those from the DFT insertion method and from the morphometric and Derjaguin approximations.

A. DFT

The DFT insertion method is described in detail in Roth *et al.* [14]. It is based on an exact result from the potential distribution theorem, for an arbitrary mixture, that expresses the effective potential between two big particles in terms of the one-body direct correlation function of the big species in the limit where the density ρ_b of that species vanishes. For DFT treatments of hard-sphere mixtures that employ the fundamental measures theory (FMT) approach [30] the calculation of the effective potential requires the computation of the density profile $\rho_s(r)$ of the small spheres in the neighbourhood of a single fixed big sphere as well as knowledge of the weight functions and the excess free energy density of the (binary) mixture [14]. The FMT must be sufficiently accurate to describe a very asymmetric binary mixture, i.e., one with small values of q, in the limit $\rho_b \to 0$. In the original DFT studies [14,18] the Rosenfeld (RF) FMT [30] was employed. In the present work we employ RF, the White Bear (WB) version [46], and its modification the White Bear Mark 2 (WB2) version [47]. These versions differ from RF in the choice of the coefficients ϕ_α entering the excess free-energy function. RF yields thermodynamic quantities that are the same as those from Percus-Yevick (compressibility) approximation, whereas WB incorporates the accurate Mansoori-Carnahan-Starling-Leland (MCSL) empirical bulk equation of state. In WB2 additional self-consistency requirements are imposed on the pressure. The consistency of the WB2 version was demonstrated in calculations of the surface tension and other interfacial thermodynamic coefficients for a one-component hard-sphere fluid adsorbed at a hard spherical surface [47]. Reference [48] provides an overview of recent developments and describes comparisons between different versions of FMT.

Boţan *et al.* [24] carried out DFT insertion method calculations as well as explicit (brute force) free-energy minimization for two fixed big spheres using different versions of FMT. These authors provide a compendium of the ingredients entering the FMT functionals as well as the thermodynamic coefficients required in the morphometric approximation, and we refer readers to Appendix B of Ref. [24] for the explicit formulas used in the present calculations. Their paper is important in pointing to the regimes where the DFT insertion method is likely to fail. In particular, for $\eta_s^r = 0.419$ and $q = 0.1$ and 0.2 there are substantial differences between the results for the depletion potential calculated by brute force and from the insertion method. At higher reservoir packing fractions the differences can be even larger. Moreover different FMTs can give rise to quite different potentials at high small sphere packings. The comparisons made by Oettel *et al.* [31] for the depletion force using the RF functional suggest that for $q = 0.05$ the insertion method is not especially accurate at $\eta_s^r = 0.314$ and 0.367. Of course, one is assuming that the brute force minimization is the more accurate method as this requires only a reliable functional for a single-component hard-sphere fluid, not one for the asymmetric mixture.

However, our present study focuses on smaller values of η_s^r than those considered in Ref. [24]. Previous studies [14, 18] showed generally good agreement between DFT insertion results and those of simulation for $q = 0.1$ and 0.2 and η_s^r typically up to 0.3. Since we are concerned primarily with investigating the depletion potential for highly asymmetrical mixtures in regimes, accessible to simulation, near the onset of fluid-fluid phase separation, we do not concern ourselves with very high values of η_s^r where the DFT insertion method is likely to be inaccurate.

Another way of viewing this DFT insertion method is that it is equivalent [14,18] to calculating the big-big radial distribution function $g_{bb}(r)$ for a binary mixture using the test particle route; i.e., one fixes a big sphere at the origin and computes the inhomogeneous density profile of the big spheres $\rho_b(r)$ by minimizing the mixture free-energy functional for this spherical geometry. Then $g_{bb}(r;\rho_b) = \rho_b(r)/\rho_b$ and the depletion potential is given by

$$-\beta W(r) = \lim_{\rho_b \to 0} \ln g_{bb}(r;\rho_b), \quad \text{for} \quad r > \sigma_b. \tag{13}$$

In Refs. [14,18], for all cases considered, it was demonstrated that a bulk packing fraction $\eta_b = 10^{-4}$ of the big spheres was sufficiently small to ensure that the depletion potential calculated from $g_{bb}(r)$ had converged to the limiting form. In a very recent paper Feng and Chapman [49] used the mixture WB theory to calculate $g_{bb}(r)$ via the test particle route. For size ratios $q = 0.1$ they report good agreement with existing simulation results [50] for concentrations of the big hard spheres as small as 0.002 and total packing fractions as large as 0.4. However, the packing fraction η_b is still too high to be appropriate for determining the depletion potential.

Roth *et al.* [14] also introduced a parameterized form for the depletion potential obtained from their DFT insertion method calculations. Their motivation was to provide an explicit form $W = 1/2(1/q + 1)\,\tilde{W}(x,\eta_s^r)$, with $x = h/\sigma_s$ and $h = r - \sigma_b$ the separation between the surfaces of the big spheres, that would be valid for a range of size ratios q and reservoir packing fractions η_s^r and therefore efficacious in studies of the phase behavior and correlation functions of binary hard sphere mixtures. The authors were influenced by the comprehensive simulation studies of Dijkstra *et al.* [4], which had employed a very simplified (third-order virial expansion) formula for the depletion potential derived in Ref. [35]. Roth *et al.* aimed to provide a formula, convenient for simulations of an effective one-component fluid, that captured both the short-range depletion attraction and the long-range oscillatory behavior of $W(r)$. Such a formula is, of course, also useful in making comparisons between theory and experimental measurements of the depletion potential. Their formula for $\tilde{W}$ consists of a third-order polynomial at small x and an exponentially damped oscillatory function at large x accounting for the correct asymptotic decay [14]. Comparisons made for η_s^r between 0.1 and 0.3 and different values of q showed that the parametrized form gave a good fit to the results of the numerical calculations. Largo and Wilding [37] employed this parametrized form in simulation studies of the (metastable) fluid-fluid critical point of the effective one-component fluid, comparing their results with those from the much simpler parametrized form used in Ref. [4].

In the present study we noticed that the parametrization in Ref. [14] did not recover the correct Asakura-Oosawa limiting behavior as $\eta_s^r \to 0$, and this restricts its regime of application. Since we are concerned with making direct quantitative

comparisons between DFT and the present simulation we performed a set of new numerical DFT insertion calculations, avoiding parametrization.

B. Derjaguin and morphometric approximations

A much used theoretical tool of colloid science is the Derjaguin approximation [51] that relates the force between two large convex bodies immersed in a fluid consisting of much smaller particles or molecules to the integral of the excess pressure of the same fluid contained between two parallel walls. In recent years there has been considerable discussion about the regime of validity of the Derjaguin approximation for our present case of a fluid of small hard spheres confined between two fixed big hard spheres or between a planar hard wall and a single big hard sphere. The reader is referred to Refs. [9,14,35,52,53]. Herring and Henderson [8,9] performed simulations for the wall-sphere case for $q = 0.05$ and $\eta_s^r = 0.3$ and 0.4, comparing their results for the depletion force with those from the Derjaguin approximation and from the DFT insertion method [14]. In the present work we perform equivalent comparisons, for the sphere-sphere case, using what we believe is much more accurate simulation data for the depletion potential.

As shown in Ref. [35] the depletion potential *difference* for hard spheres obtained from the Derjaguin approximation can be expressed succinctly as

$$W_{\rm Der}(h) - W_{\rm Der}(\sigma_s) = -\frac{\epsilon\pi}{2}(\sigma_s + \sigma_b)(\sigma_s - h) \times \left[\frac{1}{2}p\left(\eta_s^r\right)(\sigma_s - h) + 2\gamma\left(\eta_s^r\right)\right]; \quad 0 < h < \sigma_s, \tag{14}$$

where h is the separation between the surfaces, $p(\eta_s^r)$ is the pressure of the small sphere reservoir, and $\gamma(\eta_s^r)$ is the surface tension between a single planar hard wall and the small sphere fluid. Within the Derjaguin approximation the potential between a wall and a single big sphere is precisely twice that between two big spheres: ϵ is 1 for sphere-sphere and 2 for wall-sphere. Expressions for the pressure and surface tension are listed in Appendix A of Ref. [24]. Another expression for the surface tension due to D. Henderson and Plischke [54] as obtained by fitting simulation data was used in Ref. [9]. For $h > \sigma_s$ the depletion potential depends on the excess grand potential of the small sphere fluid confined in the planar hard wall slit, which must be obtained from simulation or DFT [24].

Morphometric thermodynamics [32] was developed to calculate the solvation free energy (excess grand potential) of large convex bodies immersed in a solvent. Its application to determining depletion potentials is described in Refs. [24,31], where it is shown that

$$W_{\rm Morp}(h) = -p\Delta V(h) - \gamma\Delta A(h) - \kappa\Delta C(h) - 4\pi\bar{\kappa}, \tag{15}$$

for $0 < h < \sigma_s$. Here $\Delta V(h)$ and $\Delta A(h)$ are the volume and surface area of the overlap of exclusion (depletion) zones around the big spheres (or a wall and a big sphere) and $\Delta C(h)$ is the integrated mean curvature of the overlap volume. The thermodynamic coefficients are the pressure p, surface tension γ, and the two bending rigidities κ and $\bar{\kappa}$; these four quantities are functions of η_s^r.The fourth term is the difference in integrated Gaussian curvatures between a dumbbell (4π) and two disconnected spheres (8π). For $h > \sigma_s$ the dumbbell separates into two disconnected spheres. Thus $W_{\rm Morp}(h > \sigma_s) = 0$. Explicit formulas are given in Ref. [24] for the geometrical quantities and for the four thermodynamic coefficients. Note that $W_{\rm Morp}(\sigma_s^-) = -4\pi\bar{\kappa}(\eta_s^r)$, independent of size ratio. This term is small in comparison with the others.

In order to connect with the Derjaguin approximation we invoke the colloidal limit, i.e., $q \to 0$. Then the difference

$$W_{\rm Morp}(h) - W_{\rm Morp}(\sigma_s) = -\frac{\epsilon\pi}{2}(\sigma_s + \sigma_b)(\sigma_s - h)\left[\frac{1}{2}p\left(\eta_s^r\right)(\sigma_s - h) + 2\gamma\left(\eta_s^r\right)\right] - \kappa\left(\eta_s^r\right)\pi^2\sqrt{\epsilon(\sigma_s - h)(\sigma_s + \sigma_b)/2}, \tag{16}$$

for $0 < h < \sigma_s$. Since κ is positive the morphometric approach contributes an additional attractive term, augmenting the attraction from the pressure [$\Delta V(h)$] term. Here γ is negative so the surface tension [$\Delta A(h)$] term gives a repulsive contribution to the depletion potential. The physical interpretation of the third term in Eq. (15) or (16) is of a line contribution to the effective interaction associated with the circumference of the edge of the annular wedge formed between the two exclusion spheres where the line tension is $-\kappa\pi/2$ [31]. As this term is proportional to $\sqrt{\epsilon}$ (not to ϵ) Derjaguin scaling is violated [24].

The morphometric analysis must break down in the limit $h \to \sigma_s$ where Eq. (15) or (16) predicts that the depletion force is singular, diverging as $(\sigma_s - h)^{-1/2}$. The reasons for this unphysical limiting behavior are associated with problems of self-overlapping surfaces as explained in Refs. [24,31]. However, away from this limit one might expect the elegant geometrical arguments underlying the morphometric analysis to capture the essential physics. Indeed the comparisons with brute force DFT results for the depletion force in Ref. [31] indicated rather good agreement for a range of q and $\eta_s^r = 0.314$.

In Sec. IV we compare the results of Eqs. (14) and (15) with our simulation data and with results from the DFT insertion method.

IV. RESULTS

A. Test case

We have tested the ability of the GCA to accurately determine effective potentials by applying it to the case of the Asakura-Oosawa (AO) model [33,34]. This model describes colloidal hard-spheres in a solvent of noninteracting point particles modeling ideal polymer that have a hard-particle interaction with the colloids. Although not the case of additive hard-spheres which is our primary focus in this paper, the extremely nonadditive AO model does provide a very useful test bed for our simulation methodology because the exact

form of the depletion potential is known, taking the form [34]

$$\beta W_{\mathrm{AO}}(r) = \begin{cases} -\eta_s^r \frac{(1+q)^3}{q^3}\left[1 - \frac{3r}{2\sigma_b(1+q)} + \frac{r^3}{2\sigma_b^3(1+q)^3}\right], & \sigma_b < r < \sigma_b + \sigma_s \\ 0, & r \geqslant \sigma_b + \sigma_s, \end{cases} \tag{17}$$

where σ_s is the "polymer" diameter; i.e., the colloid-polymer pair potential is infinite for $r < (\sigma_b + \sigma_s)/2$.

Simulation measurements of $g(r) \equiv g_{bb}(r)$ were performed for the AO model using the GCA for a system comprising a pair of hard spheres in a cubic box of linear dimension $L = 3\sigma$ in equilibrium with a reservoir of small particles having size ratio $q = 0.1$. Since the small particles are mutually noninteracting, the chemical potential of the reservoir is just that of an ideal gas. The depletion potential was calculated as $\beta W(r) = -\ln[g(r)]$, and the results were corrected for finite-size effects according to the procedure described in Sec. II C. In Fig. 2 we compare the results of simulations of the effective potential with the exact result. Data are shown for various values of the reservoir packing fraction. In each instance, the simulation results (symbols) are indistinguishable from the analytical form (lines) within the very small statistical errors, a finding that supports the validity and accuracy of the simulations and the procedure for correcting finite-size effects.

B. Effective potentials for additive hard spheres

We turn now to our measurements of the effective potential for highly size-asymmetrical additive hard spheres and the comparison with DFT calculations. Similarly to the case of the AO model, our simulations treat the small particles grand canonically, i.e., their number fluctuates under the control of a chemical potential μ_s^r. The value of μ_s^r is chosen to yield some nominated value of the packing fraction of small particles η_s^r in the notional reservoir. Thus the simulations require prior knowledge of $\mu_s^r(\eta_s^r)$. In principle, one could employ the Carnahan-Starling (CS) approximation [55] to estimate the requisite chemical potential. However, in tests we found this approximation to be insufficiently accurate for our purposes. For instance, taking $\eta_s^r = 0.32$ as an example, if we employ the CS value for the chemical potential, we actually measure $\bar{\eta}_s^r = 0.3195$, which, while close to the target, lies outside the range of fluctuations in η_s^r that occur in a large simulation box. In order to determine μ_s^r more accurately we therefore performed a series of accurate grand canonical simulations for the pure fluid of small hard spheres in a large box of $L = 50\sigma_s$. We then employed histogram reweighting to extrapolate to the precise values of the chemical potential that corresponds to the various values of η_s^r that we wished to study. These resulting estimates are listed in Table I.

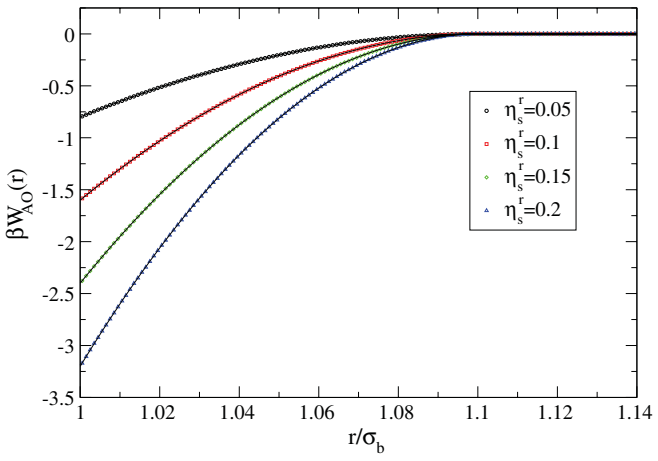

FIG. 2. (Color online) A comparison of GCA simulation measurements of the depletion potential of the AO model with the exact analytical form. The size ratio is $q = 0.1$, and data are shown for four values of the reservoir packing fraction. Symbols are results from GCA measurements of $g(r)$ for a pair of big particles, corrected for finite-size effects and transformed via $\beta W(r) = -\ln[g(r)]$. Statistical errors are smaller than the symbol size. Lines are the exact AO effective potential, Eq. (17).

Measurements of the radial distribution function $g(r)$ were made for a pair of big hard spheres in equilibrium with a reservoir of small hard spheres, for the combinations of values of η_s^r and size ratio q shown in Table II. The system size was $L = 3\sigma_b$ for $q = 0.1$, while for $q = 0.05,\ 0.02,\ 0.01$, where the range of the depletion potential is shorter, $L = 2.5\sigma_b$ was used. In all cases the depletion potential was obtained as $\beta W(r) = -\ln[g(r)]$ with corrections for finite-size effects applied as described in Sec. II C.

1. *Comparison of simulation and density functional theory results*

We now examine a selection of the measured effective potentials. Data for $q = 0.1, \eta_s^r = 0.2$ are shown in Fig. 3. Despite our use of a rather small histogram bin size of just $\delta r = 0.001$ to accumulate estimates of $\beta W(r)$, the statistical fluctuation is sufficiently small that one can simply connect the data points by lines. This allows us to better discern

TABLE I. Measured values of the reduced chemical potential $\beta\mu_s^r$ corresponding to each of the packing fractions η_s^r listed. The data were obtained by histogram reweighting the results of grand canonical simulations of hard spheres obtained at the nearby value of $\beta\mu_s^r$ predicted by the CS approximation. The simulation cell size was $L = 50\sigma_s$. The definition of μ_s^r is subject to the convention of choosing the thermal wavelength to equal the hard-sphere diameter.

η_s^r	$\beta\mu_s^r$
0.05	−1.9079(1)
0.10	−0.6770(3)
0.15	0.3923(2)
0.20	1.5105(1)
0.32	5.0472(1)
0.35	6.2659(2)

TABLE II. Combinations of particle size ratio q and reservoir volume fraction η_s^r for which we compare simulation estimates of depletion potentials with DFT predictions. Values shown in normal typeface were studied by simulation using the GCA described in Sec. II A, while those in boldface were studied using staged insertion MC as described in Sec. II B.

q	η_s^r					
0.10	0.05	0.1	0.15	0.20	**0.32**	**0.35**
0.05	0.05	0.1	0.15	0.20	–	–
0.02	0.05	0.1	0.15	–	–	–
0.01	0.05	–	–	–	–	–

differences between the simulation results and those of the DFT calculations using the insertion method, which are also included on the plot. Data for three versions of DFT are shown, namely, the Rosenfeld (RF), White Bear (WB), and White Bear 2 (WB2) functionals. Clearly for these parameters the overall agreement is very good. To quantify the extent of the accord, the two insets to Fig. 3 show a comparison in the range of separations close to hard-sphere contact (left inset) and around the first maximum (right inset). These show that near contact, WB2, fares slightly better than WB, which is in turn better than RF. Near the first maximum in the potential however, the trend is reversed, and RF has the greatest accord with the simulation data, while WB is better than WB2.

A similar picture emerges for $q = 0.05, \eta_s^r = 0.2$ as shown in Fig. 4. Although here the simulation data are not as smooth as for $q = 0.1$, the form and magnitude of the deviations from the DFT are similar. We comment later on the results of the morphometric approximation, Eq. (15).

Generally speaking, the smaller the size ratio, q, the lower the maximum packing fraction η_s^r for which we can obtain good statistics with the GCA. Data for $q = 0.02$, with $\eta_s^r = 0.1$ and $\eta_s = 0.15$, are shown in Figs. 5(a) and 5(b), respectively.

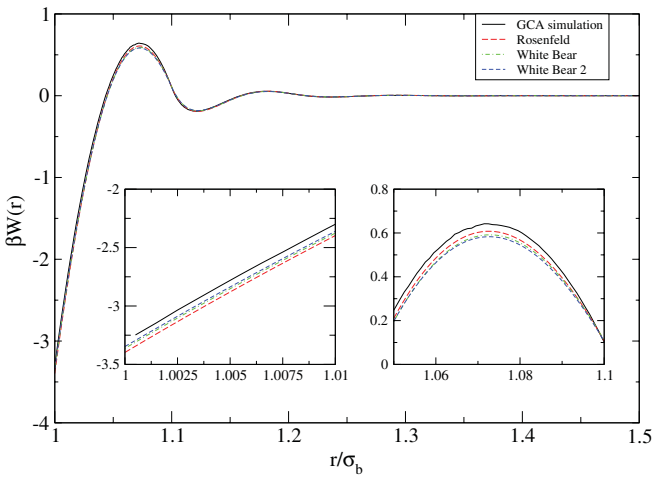

FIG. 3. (Color online) Simulation and DFT results for the hard-sphere depletion potential $\beta W(r)$ for $q = 0.1$, $\eta_s^r = 0.2$. The abscissa is the separation of hard-sphere centers expressed in units of the big particle diameter σ_b. The two insets expand the region close to hard-sphere contact (left panel) and around the first maximum (right panel).

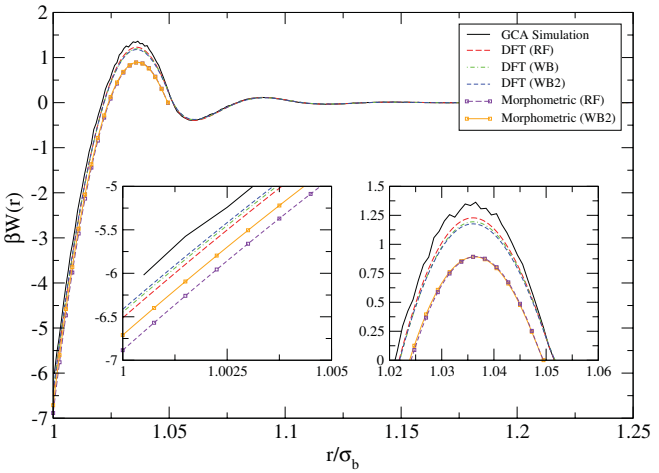

FIG. 4. (Color online) As for Fig. 3 but with $q = 0.05$, $\eta_s^r = 0.2$. Also shown are the results of the morphometric approximation Eq. (15).

For this size ratio and these (low) small-sphere packings the various versions of FMT perform very well. Data for $q = 0.01$ with $\eta_s^r = 0.05$ are shown in Fig. 6. In this extreme case the

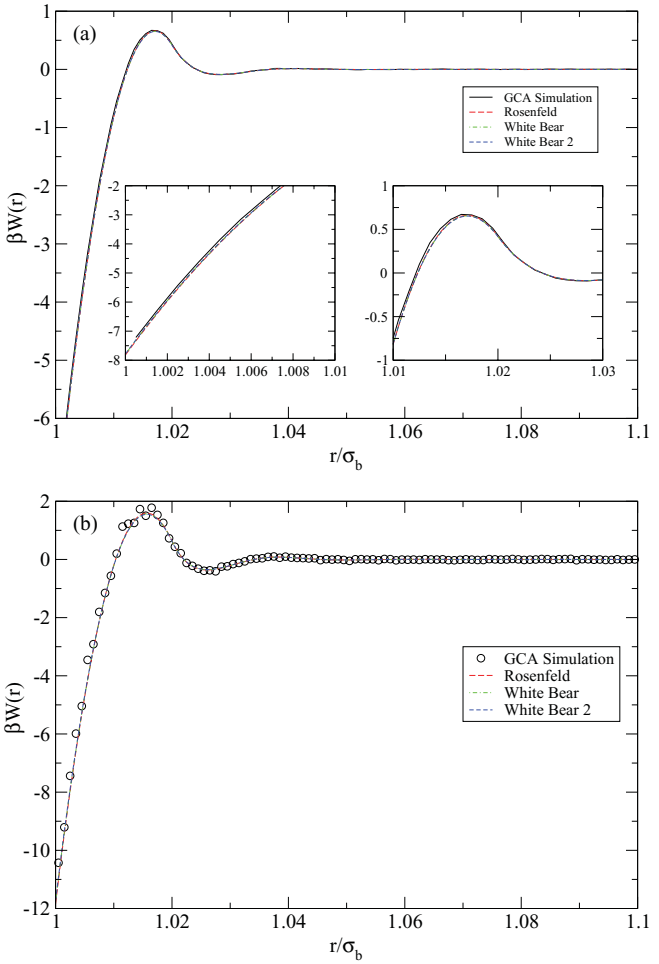

FIG. 5. (Color online) As for Fig. 3 but with (a) $q = 0.02$, $\eta_s^r = 0.1$ and (b) $q = 0.02$, $\eta_s^r = 0.15$.

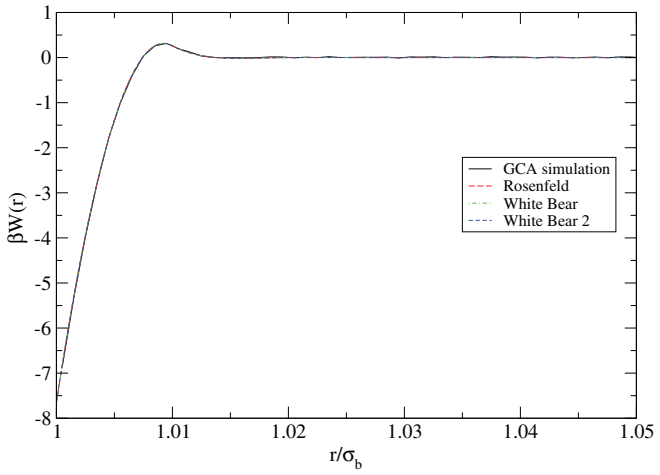

FIG. 6. (Color online) As for Fig. 3 but with $q = 0.01$, $\eta_s^r = 0.05$.

insertion DFT results are almost indistinguishable from each other and from the results of simulation. However, one should note that there is still a maximum in $W(r)$; one is not yet in the AO limit, although the contact value is close to the AO value given by Eq. (17).

For our system, the GCA is operable for $\eta_s^r \lesssim 0.2$. To go beyond this limit we have employed the staged insertion algorithm outlined in Sec. II B. Simulation results for $q = 0.1$, $\eta_s^r = 0.35$ are compared with those from DFT calculations in Fig. 7. While the simulation data are somewhat noisier, they show that in this regime, quite significant discrepancies with the DFT insertion method have emerged. The principal form of the discrepancy, i.e., DFT underestimates the height of the first maximum, is similar in form but greater in magnitude than that seen using the GCA at smaller values of η_s^r (see Fig. 3). Once again RF fares better than the two WB functionals but underestimates the first maximum by about $0.5k_BT$. Results

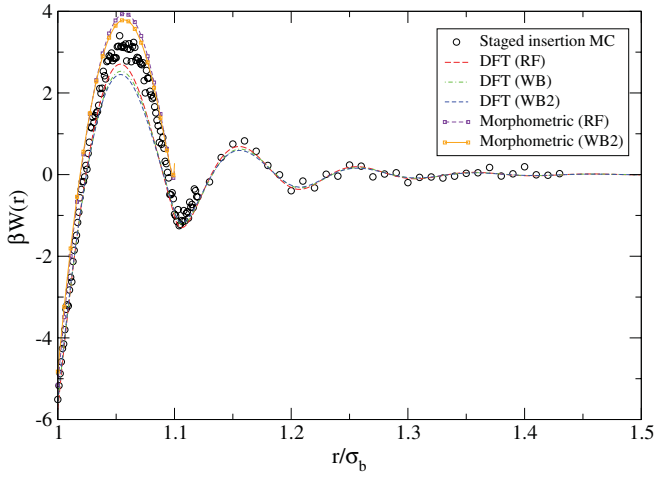

FIG. 7. (Color online) The depletion potential for $q = 0.1$, $\eta_s^r = 0.35$ obtained using the staged insertion simulation method and DFT. The simulation data points represent the results of 150 independent measurements of $\beta W(r)$ made at various fixed values of the big particle separation, though concentrated in the range $r < 1.12\sigma_b$. Also shown are the results of the morphometric approximation Eq. (15).

from the three functionals agree quite well with one another and with simulation near contact.

2. *Comparison with Derjaguin and morphometric approximations*

In this subsection we make comparisons between our simulation and DFT results with those from the approximations described in Sec. III B. Recall that the Derjaguin approximation is specifically designed to tackle small size ratios. In Fig. 4 we compare the results of the morphometric approximation Eq. (15) with those from simulation and DFT. Two sets of thermodynamic coefficient were used: RF and WB2 [24]. Both versions underestimate the maximum of the depletion potential and overestimate the magnitude of the potential at contact for $q = 0.05$ and $\eta_s^r = 0.2$. By contrast for $q = 0.1$ and $\eta_s^r = 0.35$, Fig. 7 shows that both versions of the morphometric approximation overestimate the maximum and underestimate the magnitude of the potential at contact. Figure 7 also shows a pronounced minimum for h close to σ_s. This feature is absent in both simulation and DFT. It is associated with the unphysical divergence of the line tension contribution to the depletion force arising in the morphometric treatment. Recall that W_{Morph} is zero for separations $h > \sigma_s$.

Figure 8(a) compares the depletion potential *difference* obtained from simulation and insertion method DFT for $q = 0.1$ and $\eta_s^r = 0.35$ with results from the Derjaguin approximation (where plotting the difference is the natural choice [35]) and morphometric approximations, Eqs. (14) and (15), respectively. For this value of q the packing fraction of the small spheres is sufficiently large to enter the regime where fluid-fluid phase separation might occur, as discussed below in Sec. IV B 3. Thus it is interesting to observe how well these explicit approximations perform. Similar remarks apply for $q = 0.05$ and $\eta_s^r = 0.2$, for which comparisons are presented in Fig. 8(b).

One sees in Fig. 8(a) that the Derjaguin approximation is very poor. Overall the morphometric approximations fare considerably better than Derjaguin with RF better than WB2 near the maximum. However, both morphometric versions overestimate the magnitude of the contact value by about $0.5k_BT$. Note once again the minimum close to $h/\sigma_s = 1$ for this packing fraction. The situation is clearly different in Fig. 8(b), where the Derjaguin and morphometric approximations are reasonably good; they bracket the simulation and DFT results. The two morphometric versions yield results that are very close, and even in this difference plot one sees that these fall below the simulation results both at maximum and at contact. At this smaller value of η_s^r there is no minimum visible in the depletion potential. Although plotting the difference appears to improve the level of agreement between morphometric and simulation, one should recall that it is the actual depletion potential displayed in Figs. 4 and 7, which matters, e.g., in determining $B_2(\eta_s^r)$, to which we now turn.

3. *Second virial coefficients*

While the various simulation and DFT estimates of effective potentials show generally good agreement at low η_s^r, the differences grow with increasing η_s^r, and it is natural to enquire as to the likely implications for the properties of the bulk

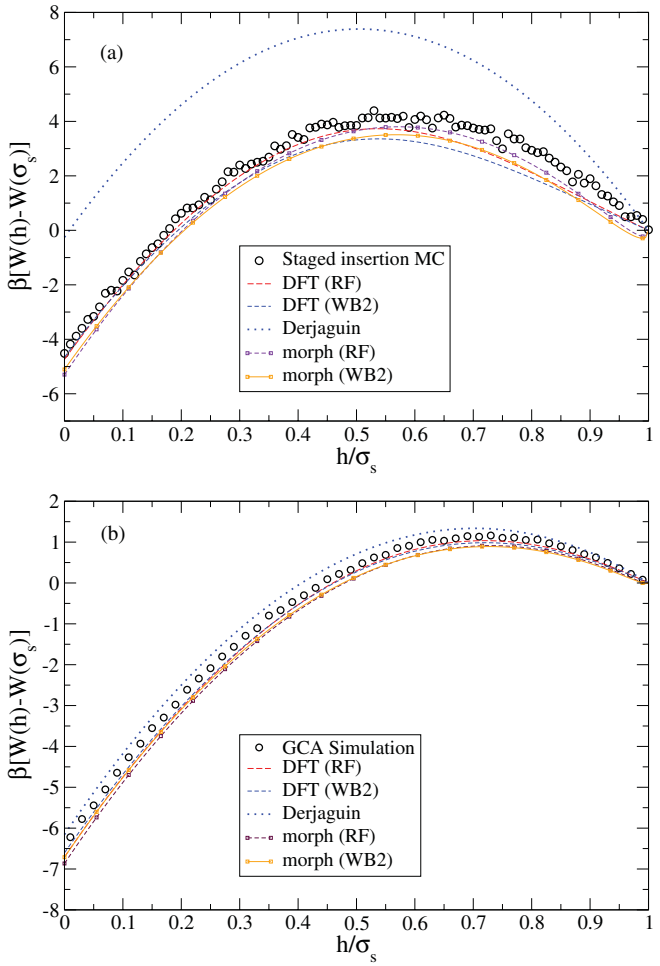

FIG. 8. (Color online) Comparison of $\beta W(h) - \beta W(\sigma_s)$ obtained from simulation and DFT for (a) $q = 0.1$, $\eta_s^r = 0.35$ (see Fig. 7) and (b) $q = 0.05$, $\eta_s^r = 0.2$ (see Fig. 4) with results of the Derjaguin Eq. (14) and morphometric approximations Eq. (15).

mixture and in particular phase behavior. A useful indicator in this regard is the value of the second virial coefficient B_2:

$$B_2 = -2\pi \int_0^\infty (e^{-\beta\phi_{\rm eff}(r)} - 1) r^2 \, dr, \tag{18}$$

where the effective pair potential is defined in Eq. (1).

Previous work by Vliegenthart and Lekkerkerker [56] and Noro and Frenkel [57] has shown that an extended corresponding states behavior applies to fluids that share the same value of B_2. Specifically, the measured values of B_2 at fluid-fluid criticality were found to be similar across a wide range of model potentials. Subsequent work by Largo and Wilding [37] examined this criterion explicitly for the case of two DFT-based hard-sphere effective potentials that had been fitted to analytical forms and parameterized in terms of the reservoir packing fraction η_s^r [4,14]. Using simulation of a single-component fluid interacting via a pair potential Eq. (1) with $W(r)$ given by these parameterized depletion potentials, the value of η_s^r at which the metastable fluid-fluid critical point occurs was determined using an accurate approach based on finite-size scaling [37,58]. Interestingly for both $q = 0.1$ and 0.05 and both choices of parameterized potentials, the value of B_2 for the depletion potential at criticality was in quantitative agreement with that of the adhesive hard-sphere model (AHS) at its fluid-fluid critical point as determined separately in simulations by Miller and Frenkel [59]. These authors report a critical value $B_2^{\rm AHS} = -1.207 B_2^{\rm HS}$, where the hard spheres' second virial coefficient $B_2^{\rm HS} = 2\pi\sigma_b^3/3$. The level of agreement was much greater than that seen for more general model potentials (such as the square well or Lennard-Jones model studied by Noro and Frenkel), suggesting that the quasi-universality of the critical point B_2 value holds particularly closely for effective potentials whose attractive piece is very short range in nature, as pertains to highly size-asymmetrical hard-sphere mixtures. Further confirmation of this has been found very recently in simulations of the AO potential where, for $q = 0.1$, Ashton [60] has found that the metastable critical point occurs at $\eta_s^r = 0.249(1)$, to be compared with the prediction $\eta_s^r = 0.2482$ based on matching to $B_2^{\rm AHS}$.

In practical terms the universality of B_2 at the fluid-fluid critical point implies that one can predict the critical point value of η_s^r for effective one-component treatments of hard-sphere mixtures at small q simply by matching the corresponding B_2 to the universal value. Conversely, it follows that comparison of B_2 values as a function of η_s^r for different potentials provides a sensitive measure of the extent to which their phase behavior differs. We have made such a comparison for effective potentials obtained from DFT, the morphometric approximation, and simulation for $q = 0.1$, 0.05, and 0.02. The results are shown in Figs. 9(a)–9(c) and demonstrate that at the two larger values of q even the relatively small differences that we observe between the DFT and simulation estimates of effective potentials could lead to significant differences in the small particle packing fractions at which fluid-fluid phase separation is predicted to occur. Specifically, for $q = 0.1$ based on this B_2 criteria, it seems that the DFT with the Rosenfeld functional underestimates the putative critical point value of η_s^r by some 13%, while the WB2 functional underestimates it by some 9%.[3] For $q = 0.05$ [Fig. 9(b)] the discrepancy between DFT and simulation has fallen to about 4%, while for $q = 0.02$ [Fig. 9(c)], the values of B_2 for the hard-sphere mixtures arising from the various DFT flavors agree very well with one another and with simulation, at least for the range of η_s^r at which bulk phase separation is expected to occur. They also agree well with the AO model, suggesting that the additive and extreme nonadditive models will have very similar phase behavior at this value of q. Recall that for $q < 0.154$ the mapping of the binary AO mixture to an effective one-component Hamiltonian, with the AO depletion potential Eq. (17), is exact, and we might also expect that for very small q the phase behavior of the full binary hard-sphere mixture, at physically relevant (small) values of η_s^r, is described accurately by the depletion pair potential we calculate here. Many-body contributions should be negligible.

[3]We note that in Refs. [36,56] an empirical (average) value $B_2^{\rm crit} = -1.5 B_2^{\rm HS}$ was used to estimate the critical point. We prefer the AHS value as an indicator of the onset of phase separation since we focus on short-range (sticky) potentials, following Largo and Wilding [37].

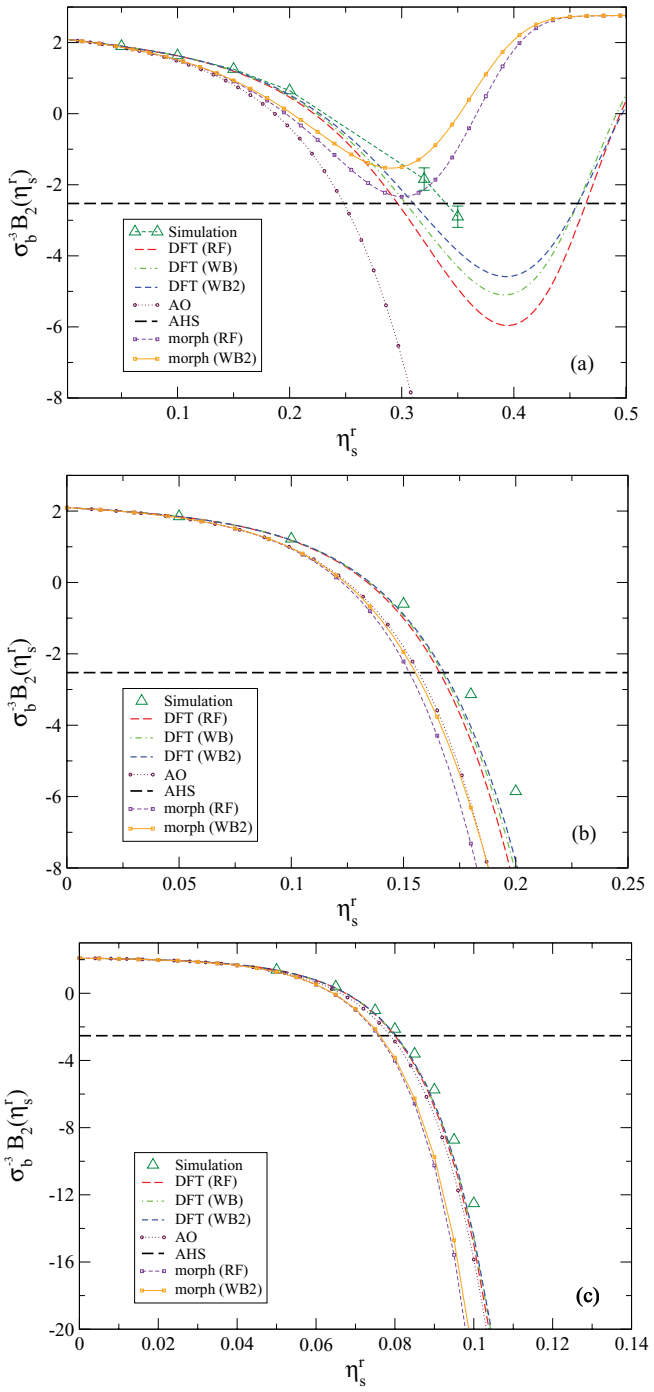

FIG. 9. (Color online) (a) Comparison of the second virial coefficient B_2 [Eq. (18)] derived from DFT and morphometric and simulation measurements of the effective potential for $q = 0.1$ and various η_s^r. The horizontal dashed line indicates the value of $B_2^{\mathrm{AHS}} = -2.527\sigma_b^3$ for which fluid-fluid criticality was found in the adhesive hard sphere model [37,59]; see text. For values of B_2 below this line, fluid-fluid phase separation is expected. Panels (b) and (c) show corresponding plots for $q = 0.05$ and 0.02, respectively. Unless error bars are shown, statistical errors in simulation data points do not exceed the symbol size.

Interestingly, the DFT data for B_2 exhibit a broad minimum with increasing η_s^r, as can be seen for $q = 0.1$ in Fig. 9(a). The same feature has previously been reported in Ref. [36]. A similar minimum occurs within the DFT for $q = 0.05$ at $\eta_s^r \approx 0.38$ (not shown in Fig. 9(b)). The origin of the upturn in the value of B_2 beyond the minimum appears to be due to the fact that the magnitude of the first repulsive maximum of $W(r)$ increases faster with η_s^r than the depth of the potential well at contact. Unfortunately we could not corroborate the authenticity of this feature via simulation because it occurs at larger values of η_s^r than are currently accessible to us. Should it prove real (rather than being an artifact of the DFT), it raises the intriguing possibility that fluid-fluid phase separation may occur only within a certain range of η_s^r.

Also plotted in Fig. 9 are the results of the morphometric approximation Eq. (15) for B_2. Like the DFT results these show minima at all q studied (though only that for $q = 0.1$ is visible in the plotted ranges). For $q = 0.1$, $B_2(\eta_s^r)$ does not cross the AHS line, implying that the theory fails to predict fluid-fluid phase separation at this size ratio. At smaller q, the agreement with simulation is better, but still poorer than DFT. It is disappointing that both versions of the morphometric approximation perform poorly for $q = 0.02$, where we find the results are substantially different from those of the AO model. The discrepancy with simulation for B_2 appears to arise primarily from a failure of the morphometric approximation to correctly predict the additive constant in the potential, as shown from the comparison of the potentials of Figs. 4 and 7 with the shifted representation of Fig. 8. While morphometric results for the depletion force [24,31] might be in reasonable agreement with DFT and simulation, any additive shift is important for B_2.

V. DISCUSSION

In summary, we have employed bespoke MC simulation techniques to obtain direct and accurate simulation measurements of depletion potentials in highly size asymmetrical binary mixtures of hard spheres having $q \leqslant 0.1$. Small particles were treated grand canonically, the value of the chemical potential being chosen to target prescribed values of the reservoir packing fraction η_s^r. The simulation results were compared with new DFT calculations (performed using the insertion method) based on the Rosenfeld, White Bear, and White Bear Mark 2 functionals. For $\eta_s^r \leqslant 0.2$ generally good agreement with simulation was found at all size ratios studied, though on increasing the packing fraction to $\eta_s^r = 0.35$ at $q = 0.1$ significant discrepancies between the various flavors of DFT and the simulation estimates were evident. In this latter regime, Rosenfeld (RF) was found to be somewhat better than the other functionals in reproducing the height of the first maximum of the effective potential, while White Bear 2 was marginally the best of the three with regard to its prediction for the contact value and for second virial coefficients.

Overall our results show that the DFT insertion method provides a reasonably accurate description of effective potentials for highly size asymmetrical hard sphere mixtures at least in the range of small particle packing fractions at which fluid-fluid phase separation is likely to occur. Indeed at $\eta_s^r = 0.35$, and $q = 0.1$ DFT was found to be more accurate than the morphometric and Derjaguin approximations, the latter providing a particularly poor prediction. This conclusion is partly at odds with that of Herring and Henderson [8,9]

who assert that both DFT and the Derjaguin approximation provide descriptions that are almost equally poor compared to simulation data (see Fig. 7 of Ref. [9], which refers to $q = 0.05$ and $\eta_s^r = 0.3$ and 0.4) and advocate in particular that neither approach should be used in the regime of "moderate" η_s^r to answer important questions such as the existence of fluid-fluid coexistence. While we concur with this assessment in the case of the Derjaguin approximation, Herring and Henderson's conclusions regarding the accuracy of DFT calculations were reached on the basis of simulation estimates for the effective potential which were not obtained directly, but by integrating measurements of the interparticle force as outlined in Sec. I A. Perhaps as a consequence, their estimates are much noisier (see Fig. 6 of Ref. [9]) than those presented in the present work and consequently, we believe, do not serve as a sufficiently reliably indicator of the accuracy of DFT, especially in the key regime where fluid-fluid phase separation might occur.

Indeed, we have investigated the likely extent of the consequences for predictions of phase behavior arising from discrepancies between theory and simulation estimates of depletion potentials via calculations of the dependence of the second virial coefficient on η_s^r. Previous simulation studies of phase behavior in single-component fluid interacting via effective potentials [37] have shown that when the potential is very short range, the onset of fluid-fluid phase separation occurs at a near-universal value of $B_2 = -2.527\sigma_b^3$. Based on this criterion, we found that compared to the effective potentials obtained via simulation in the present work, the morphometric theory provides the poorest predictions of the critical packing fraction of small particles (and fails to predict phase separation at all at $q = 0.1$). Those from DFT underestimate the critical packing fraction of small particles by about 10% for $q = 0.1$ and about 4% for $q = 0.05$. While these are significant discrepancies, we do not feel that they constitute a "qualitative breakdown" of the DFT insertion method approach as suggested by Herring and Henderson [8,9] on the basis of their simulation data, at least not in the regime where phase separation is expected. Herring and Henderson speak of a nanocolloidal regime. We interpret this as size ratios q of, say, 0.1 to 0.01. Our present study shows that this regime is amenable to accurate simulation studies up to values of the small-sphere packing fraction that are relevant for investigations of fluid-fluid phase separation and that DFT works well in this regime, the focus of the present paper. For larger values of η_s^r there are serious issues concerning the accuracy of the existing DFT approaches, and we shed no new light on this interesting but somewhat extreme regime.

Turning finally to the outlook for further work on highly size-asymmetrical mixtures, it would, of course, be of great interest to verify the existence (or otherwise) of the putative fluid-fluid critical point in the full two-component size-asymmetric hard sphere mixture. This topic remains ebullient. For example, Ref. [26] provides evidence based on integral equation studies of the binary mixture and comparison with simulation studies of the effective one-component fluid [4,37] for (metastable) fluid-fluid phase separation, and a recent paper [61], based on a version of thermodynamic perturbation theory, conjectures that additive hard spheres will exhibit fluid-fluid separation, albeit metastable with respect to the fluid-solid transition, for size ratios in the range $0.01 \leqslant q \leqslant 0.1$. Our measurements of B_2 for the depletion potentials obtained in our simulations provide predictions for the small particle packing fraction at which the critical point occurs. The accuracy of these predictions was demonstrated for an effective potential exhibiting oscillations [37] and for the (nonoscillatory) AO potential with $q = 0.1$ [60]. While this does not prove that the B_2 criterion is sufficiently robust to predict phase behavior accurately for *all* effective potentials, i.e., all size ratios, it shows that the criterion is a very powerful *indicator* for the onset of fluid-fluid phase separation. We are currently employing a grand canonical version of the staged insertion MC method [43] to investigate its usefulness in this context.

The simulation methods we develop here can be applied to any short-range potential, and it would also be of interest to examine the influence on the effective potential of adding small amounts of finite attraction or repulsion to the *bs* and *ss* interactions. This would allow us to better model real colloidal systems, where one can have a variety of interaction potentials, and where, even in systems (such as sterically stabilized PMMA) that approximate hard spheres rather well, one expects residual non-hard-sphere interactions [62,63]. Previous work [36,64] has suggested that the effects of such residual interactions may be represented in terms of a *nonadditive* hard-sphere mixture. It would be of interest to examine this proposal explicitly using accurate simulation data and DFT calculations.

ACKNOWLEDGMENTS

This work was supported by EPSRC grant EP/F047800 (to NBW). Simulation results were partly produced on a machine funded by HEFCE's Strategic Research Infrastructure fund. The authors are grateful to Martin Oettel for comments on the original manuscript and in particular on the morphometric approximation.

[1] C. N. Likos, Phys. Rep. **348**, 267 (2001).
[2] W. G. McMillan and J. E. Mayer, J. Chem. Phys. **13**, 276 (1945).
[3] L. Belloni, J. Phys. Condens. Matter **12**, R549 (2000).
[4] M. Dijkstra, R. van Roij, and R. Evans, Phys. Rev. E **59**, 5744 (1999).
[5] P. Germain and S. Amokrane, Phys. Rev. Lett. **102**, 058301 (2009).
[6] W. C. K. Poon, A. D. Pirie, and P. N. Pusey, Faraday Discuss. **101**, 65 (1995).
[7] P. J. Lu, E. Zaccarelli, F. Ciulla, A. B. Schofield, F. Sciortino, and D. A. Weitz, Nature (London) **453**, 499 (2008).
[8] A. R. Herring and J. R. Henderson, Phys. Rev. Lett. **97**, 148302 (2006).
[9] A. R. Herring and J. R. Henderson, Phys. Rev. E **75**, 011402 (2007).
[10] H. N. W. Lekkerkerker and R. Tuinier, *Colloids and the Depletion Interactions*, Lecture Notes in Physics, Vol. 833 (Springer, Berlin, 2011).

[11] D. Rudhardt, C. Bechinger, and P. Leiderer, Phys. Rev. Lett. **81**, 1330 (1998).
[12] C. Bechinger, D. Rudhardt, P. Leiderer, R. Roth, and S. Dietrich, Phys. Rev. Lett. **83**, 3960 (1999).
[13] J. C. Crocker, J. A. Matteo, A. D. Dinsmore, and A. G. Yodh, Phys. Rev. Lett. **82**, 4352 (1999).
[14] R. Roth, R. Evans, and S. Dietrich, Phys. Rev. E **62**, 5360 (2000).
[15] D. Kleshchanok, R. Tuinier, and P. R. Lang, J. Phys. Condens. Matter **20**, 073101 (2008).
[16] T. Biben, P. Bladon, and D. Frenkel, J. Phys. Condens. Matter **8** (1996).
[17] R. Dickman, P. Attard, and V. Simonian, J. Chem. Phys. **107**, 205 (1997).
[18] B. Götzelmann, R. Roth, S. Dietrich, M. Dijkstra, and R. Evans, Europhys. Lett. **47**, 398 (1999).
[19] P. Attard, J. Chem. Phys. **91**, 3083 (1989).
[20] J. Malherbe and S. Amokrane, Mol. Phys. **99**, 355 (2001).
[21] J. G. Malherbe and W. Krauth, Mol. Phys. **105**, 2393 (2007).
[22] J. Liu and E. Luijten, Phys. Rev. E **71**, 066701 (2005).
[23] S. A. Barr and E. Luijten, Langmuir **22**, 7152 (2006).
[24] V. Boţan, F. Pesth, T. Schilling, and M. Oettel, Phys. Rev. E **79**, 061402 (2009).
[25] S. Amokrane, A. Ayadim, and J. Malherbe, J. Chem. Phys. **123**, 174508 (2005).
[26] A. Ayadim and S. Amokrane, Phys. Rev. E **74**, 021106 (2006).
[27] S. B. Yuste, A. Santos, and M. L. de Haro, J. Chem. Phys. **128**, 134507 (2008).
[28] D. Goulding and S. Melchionna, Phys. Rev. E **64**, 011403 (2001).
[29] D. Goulding, Ph.D. thesis, University of Cambridge (2000).
[30] Y. Rosenfeld, Phys. Rev. Lett. **63**, 980 (1989).
[31] M. Oettel, H. Hansen-Goos, P. Bryk, and R. Roth, Europhys. Lett. **85**, 36003 (2009).
[32] P.-M. König, R. Roth, and K. R. Mecke, Phys. Rev. Lett. **93**, 160601 (2004).
[33] F. Oosawa and S. Asakura, J. Chem. Phys. **22**, 1255 (1954).
[34] S. Asakura and F. Oosawa, J. Polym. Sci. **33**, 183 (1958).
[35] B. Götzelmann, R. Evans, and S. Dietrich, Phys. Rev. E **57**, 6785 (1998).
[36] R. Roth, R. Evans, and A. A. Louis, Phys. Rev. E **64**, 051202 (2001).
[37] J. Largo and N. B. Wilding, Phys. Rev. E **73**, 036115 (2006).
[38] C. Dress and W. Krauth, J. Phys. A **28**, L597 (1995).
[39] J. Liu and E. Luijten, Phys. Rev. Lett. **92**, 035504 (2004).
[40] I. Nezbeda and J. Kolafa, Mol. Simul. **5**, 391 (1991).
[41] P. Attard, J. Chem. Phys. **98**, 2225 (1993).
[42] N. B. Wilding and M. Muller, J. Chem. Phys. **101**, 4324 (1994).
[43] D. J. Ashton and N. B. Wilding, Mol. Phys. **109**, 999 (2011).
[44] B. M. Mladek and D. Frenkel, Soft Matter **7**, 1450 (2011).
[45] A. P. Lyubartsev, A. A. Martsinovski, S. V. Shevkunov, and P. N. Vorontsov-Velyaminov, J. Chem. Phys. **96**, 1776 (1992).
[46] R. Roth, R. Evans, A. Lang, and G. Kahl, J. Phys. Condens. Matter **14**, 12063 (2002).
[47] H. Hansen-Goos and R. Roth, J. Phys. Condens. Matter **18**, 8413 (2006).
[48] R. Roth, J. Phys. Condens. Matter **22**, 063102 (2010).
[49] Z. Feng and W. G. Chapman, Mol. Phys. **109**, 1717 (2011).
[50] M. Alawneh and D. Henderson, Mol. Phys. **106**, 607 (2008).
[51] B. V. Derjaguin, Kolloid-Z **69**, 155 (1934).
[52] J. R. Henderson, Physica A **313**, 321 (2002).
[53] M. Oettel, Phys. Rev. E **69**, 041404 (2004).
[54] D. Henderson and M. Plischke, Proc. R. Soc. A **410**, 409 (1987).
[55] J. P. Hansen and I. R. McDonald, *Theory of Simple Liquids* (Academic, London, 2006).
[56] G. A. Vliegenthart and H. N. W. Lekkerkerker, J. Chem. Phys. **112**, 5364 (2000).
[57] M. G. Noro and D. Frenkel, J. Chem. Phys. **113**, 2941 (2000).
[58] N. B. Wilding, Phys. Rev. E **52**, 602 (1995).
[59] M. A. Miller and D. Frenkel, J. Chem. Phys. **121**, 535 (2004).
[60] D. J. Ashton, unpublished.
[61] P. Sillrén and J.-P. Hansen, Mol. Phys. **108**, 97 (2010).
[62] P. Germain, J. G. Malherbe, and S. Amokrane, Phys. Rev. E **70**, 041409 (2004).
[63] P. Germain, J. Chem. Phys. **133**, 044905 (2010).
[64] A. A. Louis and R. Roth, J. Phys. Condens. Matter **13**, L777 (2001).